Femtosecond Chirped Pulse Excitation of Vibrational Wave Packets in LD690 and Bacteriorhodopsin

C. J. Bardeen,† Q. Wang, and C. V. Shank*

Lawrence Berkeley National Laboratory, Berkeley, California 94720, and Department of Chemistry, University of California, Berkeley, California 94720

Received: November 26, 1997

Chirped femtosecond pulses are used to selectively excite vibrationally coherent wave packets in the ground and excited states of molecules in solution. Femtosecond chirped pump/transform-limited probe experiments on both nonreactive and reactive systems (LD690 and bacteriorhodopsin) are presented, showing that slight pulse chirps can lead to large differences in the observed amplitudes and damping times of the wave packet oscillations. By comparing the experimental data with numerical simulations based on multimode harmonic oscillator models for the molecular potential energy surfaces, we conclude that positively chirped pulses discriminate against the formation of an oscillatory ground-state component via impulsive stimulated Raman scattering, while negatively chirped pulses enhance this process. The ability to separate the relative contributions of either the ground- or excited-state vibrational coherence to the transient absorption signal by slightly modifying the phase structure of the excitation pulse enables us to obtain state-specific information about the vibrational dephasing.

Introduction

The advent of ultrashort pulse lasers has provided chemists with the opportunity to observe molecular photophysics with unprecedented temporal resolution. The achievement of optical pulses with durations as short as 4.5 fs[1,2] is made possible by the ability to experimentally control the frequency-dependent phase of the laser pulse.[3] This is because the group velocity delay (GVD) $\tau(\omega)$ of a given frequency component of the field is related to the phase via[4]

$$\tau(\omega) = \partial\phi(\omega)/\partial\omega \qquad (1)$$

For a pulse with a given spectrum, all the frequency components of that spectrum must be in phase and arrive at the same time; i.e., $\tau(\omega)$ must be independent of frequency. When $\phi(\omega)$ has no quadratic or higher order dependence on frequency, the pulse is said to be transform-limited (TL).

The ability to control $\phi(\omega)$ also provides the opportunity to put higher order phase terms on the pulse spectrum in a controlled manner. These higher order phase terms are known as chirp. Chirped pulses have been used to enhance population transfer[5−7] and to control wave packet evolution[8,9] in molecular systems. Several groups[10−13] have proposed modifying the chirp of a broad-band pulse in order to create well-defined target molecular states (e.g., a squeezed state), and such tailored wave functions may be sensitive probes of molecular dynamics.[14,15] Recent experiments have used chirped ultrashort pulses to obtain information about the time scales of electronic dephasing of molecules in solution and ultrafast carrier relaxation in semiconductors.[16,17]

In this paper we present a detailed analysis of the use of chirped femtosecond pulses to excite vibrational coherences in large molecules in solution.[18] Such coherences result in wave packet motion and oscillations in a variety of time-resolved four-wave mixing spectroscopies, including transient absorption and photon echoes. The observation of such oscillations in photochemically reactive systems has provided evidence that vibrational coherence may play a role in several important photochemical reactions.[19−21] In light of recent theoretical and experimental evidence that such vibrationally coherent photochemical reactions are possible, it is important to be able to distinguish between oscillations originating from an impulsively excited ground state and those from the excited state or from a state populated from the excited state (i.e., the photoproduct). This paper shows that the use of chirped pulses can shed some light on the electronic state of the origin of the oscillations seen in experiments on such systems. By analyzing the amplitude, phase, and damping of oscillations excited by chirped ultrashort pulses, we demonstrate that such pulses can selectively excite coherent wave packet motion on either the ground- or excited-state potential energy surface of a molecule. Experiments on the laser dye LD690 and the photoreactive system bacteriorhodopsin (BR) show how the selectivity afforded by chirped pulse excitation aids in the interpretation of the observed dynamics.

The mechanism by which we achieve this selectivity has been observed before in numerical simulations of chirped pulse excitation of CsI[22] and can be thought of as a one-photon variant of the "pump−dump" process proposed by Tannor and Rice[23] as a means to achieve selectivity in photochemical reactions. Figure 1 shows a schematic of the process that gives rise to much of the effects we observe. In the wave packet picture,[24] the first field interaction places amplitude on the excited state where it starts to slide down the potential surface. A second field interaction can either bring more amplitude up, creating population in the excited state, or it can bring the amplitude from the first field interaction back down to S_0, creating a displaced hole in the ground state.[25] In this latter case the two sequential field interactions result in an impulsive resonant Raman process that transfers momentum from the light pulse

† Present address: Department of Chemistry and Biochemistry, University of California, San Diego, La Jolla, CA 92093-0339.

S1089-5639(98)00346-6 CCC: $15.00
Published on Web 04/07/1998

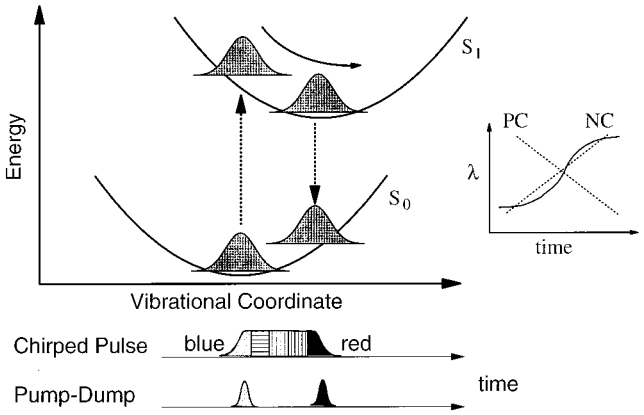

Figure 1. Schematic of the two electric field interactions that give rise to the impulsive resonant Raman process leading to ground-state wave packet oscillations, along with the frequency components as a function of time for the negatively chirped pulse that enhances this process. Shown for comparison is the two-pulse "pump−dump" sequence, which would also lead to the nonstationary ground state. The inset figure shows the evolution of the wavelength of the S_1 wave packet as a function of time (solid) and the time-dependent wavelength of negatively chirped and positively chirped pulses (dashed).

to the S_0 wave function using the S_1 state as an intermediary. Since the wave packet on S_1 is moves from higher optical frequencies to lower, the second process will be enhanced when the color components of the pulse are ordered in time so that red follows blue. Thus a negatively chirped (NC) pulse favors the creation of a nonstationary ground-state hole, while a positively chirped (PC) pulse will discriminate against the formation of the oscillating ground-state component. Although pump−probe experiments are often assumed to probe only dynamics on the excited state, a short pulse interacting with a molecular system can always induce motion in the ground state via this mechanism, introducing ambiguity into the interpretation of the observed dynamics. Chirping the pump pulse provides a way to experimentally enhance wave packet motion on either the ground or excited state and allows one to selectively probe dynamics on those states.

It is important here to distinguish between the excitation of wave packet motion, which depends on the creation of vibrational coherences, and the net amount of population transfer, which in the weak field limit is independent of the pulse chirp.[5,26] In the present experiments the pulse chirp does not affect the amount of population in either the excited state or ground state, but rather the vibrational coherence within those populations. It is these vibrational coherences that provide information on the wave packet dynamics on the electronic potential energy surfaces and which we observe in the pump−probe signal. The fact that these coherences are quite sensitive to the chirp of the optical excitation pulse shows the importance of taking the detailed nature of the excitation into account when analyzing such experiments.

Experimental Section

The laser system used to produce the ultrashort pulses in this experiment has been described before.[3,27] Sixty-femtosecond amplified CPM pulses are used to generate continuum in two different single-mode fibers, one of which is compressed in the usual manner with gratings and prisms, yielding an ultrashort (10-fs) probe pulse. The output of the other fiber travels through a grating pair, a broad-band dye amplifier,[28] and then a set of prisms, resulting in a pulse width of 12 fs. The amplified short pulse is slightly longer than the unamplified probe pulse owing

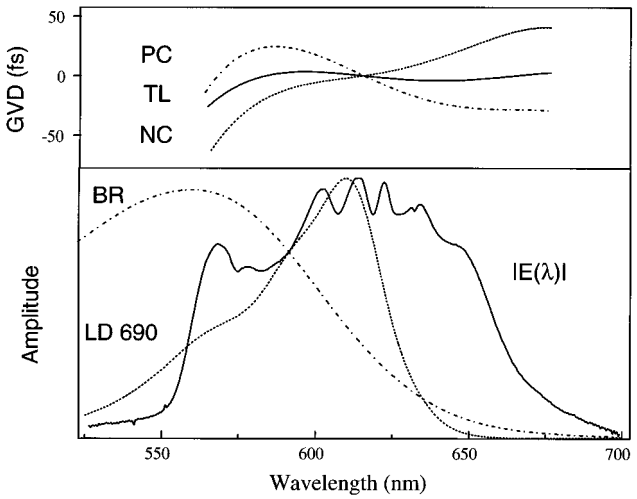

Figure 2. (Top) Measured group velocity delay times across the spectrum for grating separations corresponding to PC, TL, and NC pulses described in the text. (Bottom) Experimentally measured $|E(\lambda)|$ spectrum of the 12-fs pulse, along with the absorption spectrum of LD690 in methanol (dashed) and bacteriorhodopsin (dot-dashed).

to the limited gain bandwidth of the amplifier, which results in a narrower spectrum. The pulse energies are on the order of 0.5 nJ, where the signal was found to be linear with pump intensity. Experiments on LD690 are performed on a flowing jet of the dye dissolved in methanol, with a probe transmission of at least 50%, while those on BR used a buffered aqueous solution[27] flowed in a 200-μm path length sample cell and continuously illuminated to ensure that it remains in its light-adapted form. The pump probe signals are detected several ways: single-wavelength detection was accomplished by spectrally filtering the probe after the sample with a monochromator or interference filter and using lockin detection in conjunction with differential amplification to collect the pump-induced transmission. Alternatively, entire spectra were obtained by taking the probe beam and putting it into an optical multichannel analyzer, which detects all wavelengths simultaneously.[29]

The chirp of the pump pulse is modified by changing the separation of the pulse compression gratings. Although this affects mainly the linear chirp,[4] higher order terms in the phase structure of the pulse can be affected too, and it is important to have a way of measuring the actual phase of the pulse. This is done by cross-correlating the 60-fs narrow band pulse with the 12-fs pulse in a 100-μm KDP crystal and analyzing the spectrum of the upconverted signal.[3,30] By selecting the right mixing frequency, we can determine the arrival time of a given frequency component of the original broad-band pulse. By fitting the experimentally determined $\tau(\omega)$ to a polynomial, we can easily obtain the frequency-dependent phase from eq 1. Figure 2 shows a typical pulse spectrum $|E(\lambda)|$, the absorption spectra of LD690 and BR, and typical measured frequency delays $\tau(\lambda)$ for different grating settings. A linear least-squares fit to the data yields quadratic phase terms $\Phi''(\nu)$ of -6109, -214, and $+5179$ fs^2, respectively, which determine the linear chirps. This quadratic phase term varies linearly with grating separation, as predicted.[4] The intensity autocorrelation widths are 43, 19, and 57 fs, respectively, which correspond to pulse widths of 28, 12, and 37 fs, assuming a sech^2 intensity profile. We found that, for a given magnitude of $\Phi'(\nu)$, positive and negative chirps did not give the same pulse widths owing to the asymmetric power spectrum. Also, even the shortest pulse is not really transform-limited, which would result in a flat plot of GVD vs wavelength, but has residual cubic structure (this

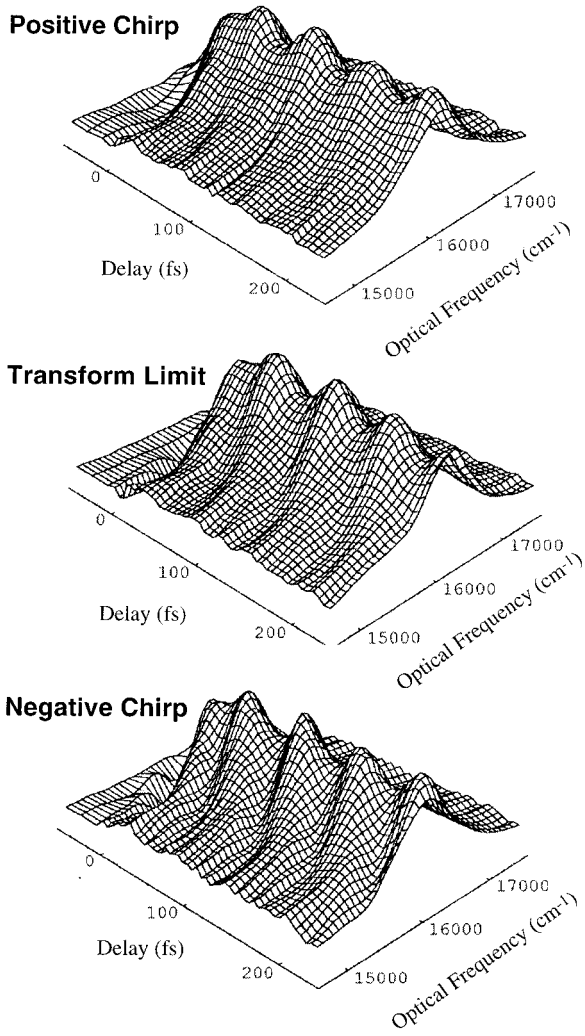

Figure 3. Time-resolved absorption spectra of LD690 in methanol excited by (1) a positively chirped pulse with an intensity autocorrelation width = 19 fs (top), (2) a transform-limited pulse with an intensity autocorrelation width = 12 fs (middle), and (3) a negatively chirped pulse with an intensity autocorrelation width = 25 fs (bottom). The vertical axis corresponds to the normalized transmission change, $\Delta T/T$.

has been observed previously for compressed pulses[31]). We refer to the shortest duration pulse as transform-limited (TL) for the sake of convenience.

Results

1. LD690. Figure 3 shows the dynamic absorption spectra of LD690 with NC, TL, and PC pump pulses. The pulse widths are 25, 12, and 19 fs, respectively. The approximately 60-fs oscillations in the induced transmission correspond to LD690's dominant 586-cm^{-1} mode and have been observed before.[32] The oscillations are due both to wave packet motion of the population impulsively created on the excited-state potential and to the nonstationary "hole" left behind in the ground state and are seen at all wavelengths. The behavior of the oscillations can be roughly classified according to the spectral region of the detected wavelength. The three regions we will be concerned with are the region to the blue of the absorption maximum (570−600 nm), the region around the absorption maximum (600−620 nm), and the red end of the spectrum (620−680 nm).

The most dramatic effects are seen in the red part of the spectrum: Figure 4 shows the pump−probe signal at 640 nm detected with a monochromator and lockin, along with the

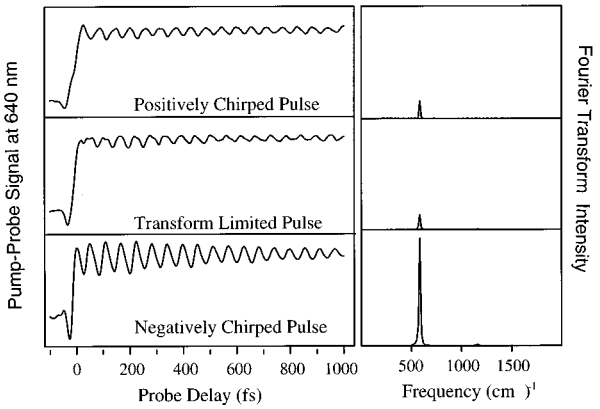

Figure 4. Experimental pump−probe signal for LD690 at 640 nm: top trace = positively chirped pulse, autocorrelation width = 33 fs; middle trace = "transform-limited" pulse, autocorrelation width = 12 fs; bottom trace = negatively chirped pulse, autocorrelation width = 20 fs. Also shown are the Fourier power spectra of the oscillatory component.

Fourier power spectra of the oscillations. To obtain the spectra, we first Fourier filter the data to remove all high-frequency oscillations. This smoothed component is then subtracted from the original data, and the result is divided by the smoothed component, so that the oscillations are normalized to the total signal level. For the data shown here, the PC pulse width is 33 fs, the TL pulse width is 12 fs, and the NC pulse width is 20 fs, and although the measured pulse widths are different, the size of linear chirp on the pulses is very similar, as was explained in the Experimental Section. In all three spectra we see a large 586-cm^{-1} peak and a trace of a broader peak at about 1170 cm^{-1}, which corresponds to the second harmonic of the 586-cm^{-1} mode. Any other peaks that might be present are within the noise level. As we put negative chirp on the pulse, the oscillations at 640 nm are first enhanced, with a maximum enhancement occurring at a chirp corresponding to a pulse about twice as long as the TL pulse (this maximum is the NC case shown in Figure 4) and are then slowly washed out as the pulse gets longer. At the maximum the 586 cm^{-1} peak from the NC data is almost a factor of 5 larger than that of either the TL or PC data. By moving the grating in the opposite direction and putting positive chirp on the pulse, we find that the oscillations are only diminished, never enhanced. The region around the absorption maximum, 610 nm, exhibits oscillations that are far less dependent on the chirp, although their amplitude does decrease with both positive and negative chirp. At 600 nm we see an opposite trend from the 640-nm data—a slight enhancement as we chirp the pulse positively, while negative chirp results only in smaller oscillations. To the blue edge of the probe spectrum, around 580 nm, we see that the oscillations are lessened by both positive and negative chirp. In summary, by looking at the extent to which the 586 cm^{-1} mode modulates the pump−probe signal, we find that chirping the excitation pulse can have a profound effect on the dynamical evolution of the population. The fact that, for a given pulse width, positively or negatively chirped pulses yield very different signals shows that these effects are not just due to the temporal broadening of the pulses.

2. Bacteriorhodopsin. Various probe wavelengths were detected, but our analysis will concentrate on the signal detected at 656 nm, close to the peak of the photoproduct absorption. Figure 5 shows the experimental differential transmittance at this wavelength, and we see the rapid growth of the induced absorption as the molecule isomerizes, on which are superimposed are the oscillations resulting from wave packet motion

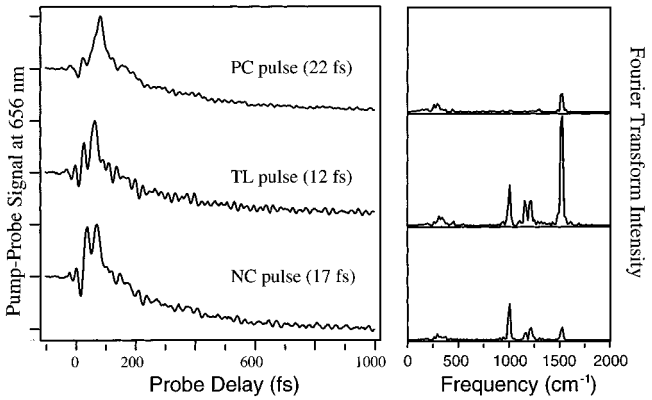

Figure 5. Experimental pump−probe signal detected at 656 nm for BR with NC, TL, and PC pump pulses with pulse widths (assuming $sech^2$ pulse shapes) of 17, 12, and 22 fs, respectively. The Fourier power spectra of the time-dependent oscillations are shown at right.

in S_0. Next to the pump−probe traces are the normalized Fourier power spectra of those oscillations. The middle trace, corresponding to the TL pulse, is similar to that obtained previously[27] and exhibits four strong peaks in the high-frequency part of the Fourier spectrum. All these peaks correspond to modes observed previously in resonant Raman experiments. Also shown are the traces and Fourier transforms for PC and NC pulses. In the case of BR we cannot chirp the pulse very much before we wash out the oscillations completely. The high-frequency vibrations have such short periods, 20−30 fs, that we cannot adjust the gratings very far before the pulse duration is longer than the period and we lose the ability to impulsively excite the mode. Even with these light chirps, we do see an effect, especially for the modes around 1000−1200 cm^{-1}. A PC pulse completely extinguishes the peaks in this region, while they are still present in the NC data. The 1530-cm^{-1} mode is decreased by about the same amount by either chirp. We do not, however, see any enhancement of BR's oscillations by applying a NC pulse, unlike in LD, where the Fourier peak increased by a factor of roughly 5. Note that the low-frequency structure around 250 cm^{-1} is largely unaffected by these pulse chirps.

Calculations and Discussion

As mentioned in the Introduction, we believe the main effect of chirping the pulse is to change the amount of ground-versus excited-state contribution to the oscillations. One way to distinguish between the two would be if the vibrational frequencies in S_0 and S_1 are different. Joo and Albrecht have analyzed their four-wave mixing experiments in terms of a 586-cm^{-1} ground-state vibration and a 571-cm^{-1} excited-state vibration.[33] If this were the case, one could distinguish ground- and excited-state contributions to the pump probe signal by using the Fourier transform of the data alone. Our resonance Raman measurements, however, are consistent with the 571-cm^{-1} mode being ground state in origin—it has a narrow line width, and its relative intensity does not depend on the excitation power. Fourier transforms of long-time traces did not turn up any new frequencies besides those already seen in the resonance Raman measurements, and the 571 cm^{-1} shows up as a slight shoulder on the 586-cm^{-1} peak. Since there is no evidence of new vibrational frequencies in S_1, in order to model the data we make the assumption that the excited-state PES is identical to the ground-state one except for a mode-dependent shift of the potential energy minima.

The assumption that the excited state is merely a displaced version of the harmonic ground state makes it straightforward to numerically simulate the data. The differential pump−probe signals are related to the third-order polarization $P^{(3)}(\omega)$ via

TABLE 1

ω (cm^{-1})	D	ω (cm^{-1})	D	ω (cm^{-1})	D
303	0.32	1143	0.09	1416	0.20
571	0.43	1159	0.10	1523	0.16
586	0.90	1172	0.20	1540	0.14
734	0.28	1244	0.11	1553	0.14
813	0.09	1344	0.23	1568	0.15
1130	0.14	1365	0.13	1662	0.35

$$\Delta T/T \propto \chi^{(3)}(\omega) = P^{(3)}(\omega)/E_{\text{probe}}(\omega) \quad (2)$$

To obtain $P^{(3)}(\omega)$ we must numerically integrate the four time correlation functions that result from solving the time-dependent Liouville equation perturbatively to third order[34,35]

$$P^{(3)}(t) = (i/\hbar)^3 \int_{-\infty}^{t} dt' \int_{-\infty}^{t'} dt'' \int_{-\infty}^{t''} dt''' \, E(t') \, E(t'') \, E(t''') \times \sum_{i=1}^{4} R_i(t - t', t' - t'', t'' - t''') \quad (3)$$

where R_i can be written as the product of harmonic oscillator linear response functions,[34] for instance

$$R_1(t_1, t_2, t_3) = \exp[g(t_1) + g^*(t_2) + g^*(t_3) + g(t_1 + t_2 + t_3) - g(t_1 + t_2) - g^*(t_2 + t_3)] \quad (4)$$

The line shape function $g(t)$ is evaluated for undamped harmonic oscillators for the case of intramolecular vibrational modes and as a stochastic broadening function to take solvent effects and dephasing into account

$$g_{\text{intra}}(t) = (D^2/2)[(\bar{n} + 1)(e^{-i\omega t} - 1) + \bar{n}(e^{i\omega t} - 1)] \quad (5)$$

$$g_{\text{inter}}(t) = i\lambda \int_0^t dt' \, M(t') + \Delta^2 \int_0^t dt' \int_0^{t'} dt'' \, M(t'') \quad (6)$$

The intramolecular parameters, namely 18 harmonic modes with frequencies (ω) and dimensionless displacements (D) derived from resonance Raman data, can be found in Table 1. The intermolecular parameters, including the fluctuation width Δ and the solvation correlation function $M(t)$, are those used before to calculate photon echo signals for LD690 in methanol.[36] The electric field of the pump pulse is a Fourier transform of the magnitude of experimentally measured pulse power spectrum multiplied by a frequency-dependent phase function derived from the cross-correlation measurements. Specifically, the spectrum in Figure 2 shows $|E(\lambda)|$, while a cubic polynomial was fit to the GVD data. These calculated pulses reproduced the shape of the experimentally measured pulse autocorrelations and cross-correlations to within 10−20%. The probe pulse was taken to be an 8-fs truncated Sinc function[35] whose spectral width matched that of the experimentally measured probe spectrum. The calculations in this case are fairly insensitive to the probe pulse as long as the pulse duration and spectral width do not change significantly.

The calculations confirm the intuitive picture presented in the Introduction: a negatively chirped pulse produces an enhancement of the oscillatory motion of the ground-state hole wave packet, which is manifested in the time-dependent absorption of the molecule. A positively chirped pulse, on the other hand, decreases the oscillatory component of the ground state relative to the TL case. Figure 6 shows the calculated

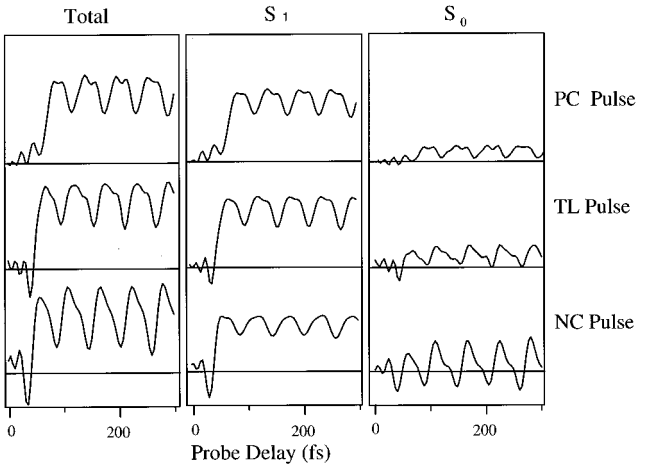

Figure 6. Calculated pump−probe signal of LD690, using the molecular parameters from Table 1 and the pulse spectrum and chirps shown in Figure 2, with the decomposition into S_0 and S_1 contributions.

signal at 640 nm along with its decomposition into ground- and excited-state components. As in the experiment, the largest effect is seen in this spectral region, with the ground-state contribution greatly increasing with the negative chirp and manifesting itself as a deeper modulation of the total signal. The excited-state contribution is slightly degraded by both positive and negative chirp because the longer excitation event broadens the wave packet.

Another comparison of theory and experiment is shown in Figures 7 and 8, which plot the frequency-resolved Fourier power spectra of the normalized oscillations of the experimental and calculated signals for PC, TL, and NC pulses. Note that in these figures both axes are in units of frequency, one being the optical probe frequency and the other being the molecular vibration frequency. The experimental values were obtained from the data as described above for Figure 5, while the calculated ones result from the calculations described above and then repeating the procedure used for the experimental data. Only the first 300 fs of data was Fourier-transformed in order to avoid complications from different damping times for different chirps (discussed below). The absolute magnitudes of the experimental and calculated Fourier transforms are not in good agreement, with the calculated amplitudes being consistently larger by up to a factor of 3, depending on the probe wavelength. We concentrate on trends across the spectrum and the qualitative agreement between theory and experiment, which should indicate whether our calculations capture the basic physics of the process. The agreement is best for the case of NC pulse excitation: both theory and experiment show a very large enhancement of the oscillations starting at around 610 nm and obviously extending well outside of the probe's spectral window. In both Figures 7 and 8 the magnitude of these oscillations is the largest seen for any pulse, modulating the transient absorption by 50% or more. One discrepancy is that the calculation predicts that a significant second harmonic of the 586-cm^{-1} mode should be visible at the low-frequency side of the window, whereas experimentally this component is not nearly so pronounced. Our expectation that a PC pulse excites mostly excited-state wave packet motion is confirmed by the observation of a strong minimum in the Fourier amplitude seen in both the calculated and experimental signals for positive chirp. The experimental minimum occurs at about 635 nm, close to the maximum of the steady-state fluorescence spectrum in methanol, which corresponds to the bottom of the S_1 potential well, according to our displaced harmonic oscillator model. Since the wave packet travels through this region twice per period and also broadens at the bottom of the well, the S_1 oscillations are washed out in this region and a minimum in their amplitude is observed.[20,35] Neither the NC nor the TL pulse data show such a minimum because in these cases there is a significant contribution from motion on S_0. Theory and experiment for TL pulse data show good agreement in the low-frequency half of the probe spectrum, but the data also shows an equally large Fourier magnitude to the high-frequency side, which is absent from the calculated signal. In fact, both the TL and the PC pulse data show a large oscillatory component extending far to the blue, while the calculated signals suggest that it should die off around 17 000 cm^{-1}. Overall, however, the agreement between experiment and calculation is fairly good, especially considering that the system being modeled is a large, complicated organic molecule in a room-temperature molecular liquid.

In addition to the amplitude of the oscillations, we can also determine their wavelength-dependent phase. Since the 586-cm^{-1} mode has a period of about 60 fs, a delay of 60 fs corresponds to a change in phase of 2π. Figure 9 shows the relative delay of the oscillations as a function of probe wavelength for NC, TL, and PC pulses, along with the calculated wavelength-dependent delays. This data was derived from the OMA measurements, where all wavelengths were detected simultaneously in order to eliminate the possibility of zero drift in the delay stage. For both positively chirped and TL pulses, the oscillations in the red end of the spectrum are approximately 180° (about 30 fs) ahead of those in the blue. Furthermore, in the PC pulse data this 180° phase shift occurs very close to the observed null in the amplitude of the oscillations. The null and phase shift are consistent with the observed oscillations being due mainly to coherent motion on the S_1 state, as the wave packet travels from high to low optical frequencies (on a time scale of 30 fs) where the oscillations are highly visible, through S_1 minimum where the phase shifts and the oscillations are washed out. For both the PC and TL excitation, the oscillations are dominated by wave packet motion on S_1, which results in the usual 60-fs round trip time as the population moves from the absorption region out to the red and then back again. Intuitively, the oscillations in the red will be 180° (30 fs) out of phase with those in the blue. When the oscillations excited by a NC pulse are analyzed, we see that there is a phase shift of about 270° between the blue and red edges of the spectrum, owing to the significant ground-state motion. Calculations show that the large phase difference is due to this ground-state component, while the excited-state component behaves as in the PC and TL cases. Referring back to Figure 1, we offer the following intuitive explanation of the extra phase shift. As the S_1 wave function moves to the red, some is pulled down to create the S_0 nonstationary hole. The S_0 wave function propagates briefly in the same direction as the S_1 wave function, but the slope of S_0 resists this motion and eventually it reverses direction and goes back toward the blue. This process results in a broad ground-state hole that does not evolve in the same intuitive way as do the more or less Gaussian wave packets on S_1. The ground-state hole undergoes a sort of breathing motion, so that modulations on the edges of the spectrum occur closer together in time than they would if they were due to a classical wave packet sloshing back and forth.

The last aspect of the observed oscillations we analyze are their damping times, which is accomplished by using a single-value-decomposition method[37] to analyze the oscillatory part of the data. This method assumes the data can be fit with a set

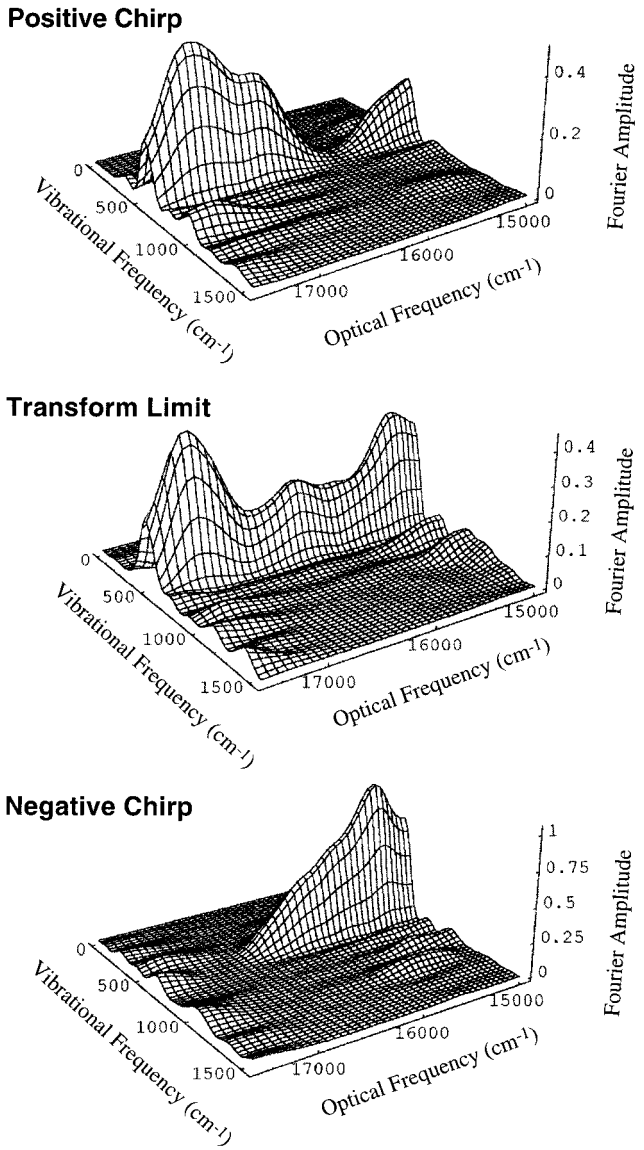

Figure 7. Normalized Fourier power spectra of the data for LD690 shown in Figure 3, after applying a weak smoothing algorithm to remove high-frequency noise components. The pulses used are (1) a positively chirped pulse with an intensity autocorrelation width = 19 fs (top), (2) a transform-limited pulse with an intensity autocorrelation width = 12 fs (middle), and (3) a negatively chirped pulse with an intensity autocorrelation width = 25 fs (bottom). The vertical axis is the Fourier amplitude of the pump-induced molecular response at a given vibrational frequency, detected at a given optical frequency. Note that the vertical scale for the negatively chirped pump pulse is different from that of the transform-limited and positively chirped pulses.

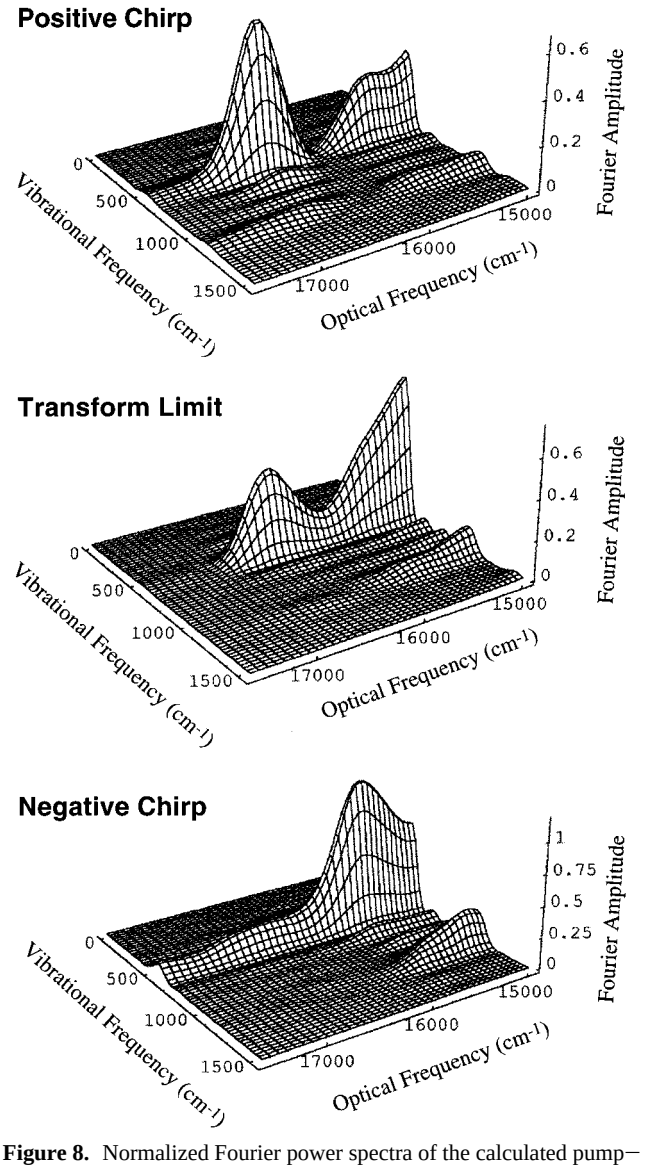

Figure 8. Normalized Fourier power spectra of the calculated pump−probe signals using the experimental pulses from Figure 2 and a multimode displaced harmonic oscillator model for LD690. Top = PC pulse, middle = TL pulse, bottom = NC pulse. The vertical axis is the Fourier amplitude of the pump-induced molecular response at a given vibrational frequency, detected at a given optical frequency. Note that the vertical scale for the negatively chirped pump pulse is different from that of the transform-limited and positively chirped pulses.

of exponentially damped sinusoids, which may not be the case in nature if the vibrational relaxation is non-Markovian or if a single frequency has multiple relaxation times. The numbers obtained from this analysis should therefore not be taken as absolute determinations of the vibrational dephasing times, but as approximate values that illustrate the trend with different probing wavelength and chirp. The most dramatic chirp effect is seen in the blue region of the spectrum this time. Figure 10 shows the oscillations at 580 nm, where a NC pulse yields essentially undamped oscillations, while the TL pulse excites oscillations that decay on the order of a picosecond, and a PC pulse results in oscillations with an even faster decay time of about 0.8 ps. Again, the oscillations at 610 nm are less sensitive to the chirp, although there is a trend toward faster decays with positive chirp. At 640 nm the situation is the reverse of 580 nm: a positively chirped pulse excites oscillations with a significantly slower decay time (roughly a factor of 2) than those caused by a TL or negatively chirped pulse. At 670 nm the situation is similar to that at 640 nm. Negatively chirped and TL pulses yield oscillations with approximately the same decay time, while positively chirped pulses result in a slower decay. In conclusion, an analysis of the decay times of the oscillations shows at least one clear trend: negative chirp yields fast-decaying oscillations in the red, while positive chirp yields fast decays in the blue. Figure 11 summarizes these decay times and illustrates the regions of the potential energy surfaces interrogated by each probe wavelength.

A qualitative explanation of the data is as follows. There is a large body of work on vibrational relaxation in polyatomic molecules[38] that suggests that higher-lying vibrational states undergo faster relaxation. Thus in the negatively chirped case, where we are dominated by the ground-state contribution, we see a fast damping in the red part of the spectrum (corresponding

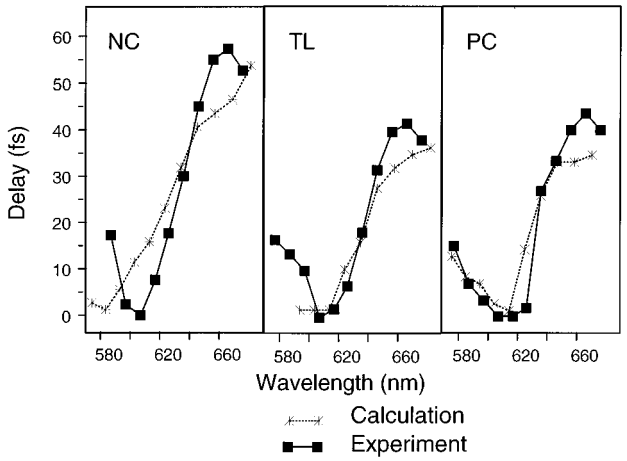

Figure 9. Wavelength dependence of the phase of the oscillations for LD690 comparing the experimental data (solid) with the calculated (dashed) delays of the 586-cm^{-1} oscillation. 60 fs = 2π phase shift.

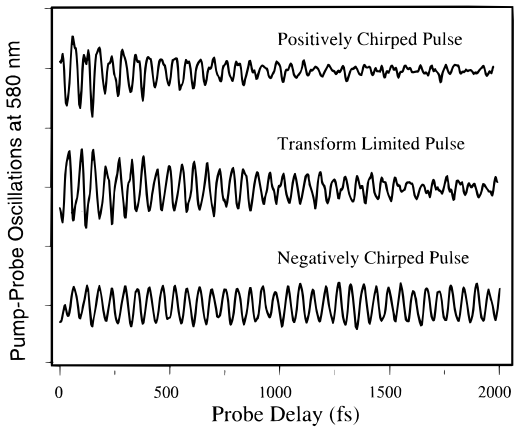

Figure 10. Different decays of the oscillatory component of the experimental pump−probe signal of LD690 at 580 nm using PC, TL, and NC pump pulses.

	Damping Times (ps)		
λ_{pr}	NC	TL	PC
580	>10	1.1	0.8
610	2.1	1.3	0.9
640	1.0	1.5	3.3
670	1.0	0.9	1.1

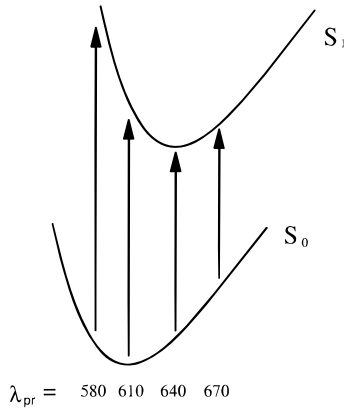

Figure 11. Dependence of the damping time of the oscillations on pulse chirp and probe wavelength for LD690.

to coherences involving higher-lying states in S_0) while the oscillations in the bluer region suffer much less damping, since they involve lower-lying states and motion closer to the ground-state minimum. The signal at 580 nm does not correspond to the ground-state minimum, but if the well is anharmonic then 580 nm will be closer to the ground-state minimum than 640 nm. As discussed above, the signal at 610 nm is dominated by the excited-state oscillations even in the case of NC excitation and will not give a good indication of the ground-state damping. Both the TL and especially the PC pulse data should be

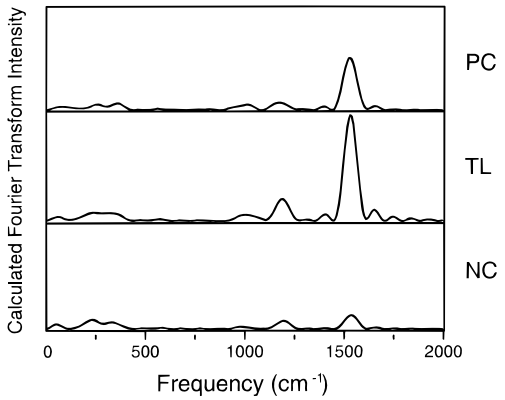

Figure 12. Fourier power spectra of the calculated signal of BR for the pulses and probe wavelength shown in Figure 5.

dominated by the excited-state wave packet motion. Here the fast damping at 580 nm is due to coherently excited higher-lying vibrational states in the S_1 vibrational manifold, now that the S_0 motion is less pronounced. There is also fairly rapid damping of the oscillations out at 670 nm, which is past the fluorescence peak and also corresponds to coherences between higher-lying vibrational states in S_1. The relatively slow damping at 640 nm, close to the excited-state PES minimum as inferred from the steady-state fluorescence peak at 635 nm, is again most likely the result of wave packet motion close to the bottom of the potential well having a longer dephasing time. A summary of this data is that, for the 586-cm^{-1} mode, vibrational dephasing for low-lying states is roughly 3 ps in S_1 and at least 10 ps in S_0, while both S_0 and S_1 show dephasing times of about 1 ps for higher-lying states. It is interesting to note that if this interpretation is correct, the vibrational dephasing rate depends on the region of the potential well the wave packet samples as well as the given electronic state.

The analysis of the chirped pulse excitation of BR is considerably more complicated than for LD. The fast movement of BR's excited-state population out of the Franck−Condon region toward the crossing point where the photoproduct is formed has been found to occur on a time scale of 200 fs.[39] The rapid disappearance of the S_1 population from the optical spectrum means that oscillations observed on a longer time scale must result from the ground state or from a coherently formed photoproduct. A careful comparison of pump−probe data with calculations based on resonant Raman data[27] has shown that ground-state oscillations in the red can be attributed to the impulsively excited ground state, and we hoped to be able to make the same determination based only on chirping the excitation pulse. The fact that we manage to kill most of BR's oscillatory component by putting a slight positive chirp on the pulse implies that we are at least partially successful in our attempt to use chirp to turn off the ground-state component. The Fourier power spectrum of a full calculation of the 656-nm signal is shown in Figure 12, and comparing this to the data in Figure 5 we see that the calculation underestimates the magnitude of the 1000 cm^{-1} peak in the TL and NC data and also predicts that the 1530-cm^{-1} mode should be much larger in the PC data than in the NC data, whereas experimentally they are of similar magnitude. The reasons for the qualitative discrepancies between theory and experiment are unclear but may be the result of modeling a reactive (and thus very anharmonic) excited state as a collection of displaced harmonic oscillators. A calculation of the same system using the linearly chirped Gaussian pulse mentioned previously showed almost complete suppression of the ground-state oscillations in the PC

calculation, including those from the 1530 cm^{-1} mode, implying that our inability to achieve this experimentally is due at least in part to the nonideal pulse shape. But even the Gaussian pulse showed no NC enhancement, and it may be that an even shorter pulse is needed, which can be both chirped and short enough to impulsively excite these higher frequency modes. The fact that the 1000-cm^{-1} peak does not disappear as quickly with negative chirp as do the higher frequency peaks suggests that some competition between chirp rate and overall pulse width is indeed occurring.

The phenomenon of a linear chirp enhancing or suppressing ground-state wave packet motion should be general and not specific to the case of displaced harmonic oscillators. Any optical transition creates a vibrational wave packet with maximum potential energy that subsequently evolves to a lower point on the PES and thus to a lower optical transition frequency. Another point is that this Raman-type process relies on two field interactions separated in time. During the period between interactions, the system is in a coherent superposition of ground and excited electronic states and hence will be subject to electronic dephasing processes, referred to as T_2. These effects will therefore be enhanced in a system with a longer electronic dephasing time, while a very short T_2 will tend to negate the chirp effects. Calculations and preliminary experiments on the molecule Nile Blue, which has a faster effective electronic dephasing time than LD690,[32] show less of an enhancement effect. Finally, it is important in these calculations to take the actual phase structure of the pulse into account. Figure 2 shows that these pulses have significant higher order chirp, and these higher order terms keep us from doing a better job of selective excitation. Calculations using Gaussian pump pulses with purely linear positive chirp showed more effective elimination of the ground-state contribution to the oscillations, and it is an open question whether there is an optimum pulse shape that can turn off the S_0 component while still appreciably exciting the S_1 component.

Conclusions

By analyzing the variation of the wavelength-dependent amplitude, phase, and damping times of the oscillations in the pump−probe signal, we have shown how modifying the phase properties of the excitation pulse can selectively excite wave packet motion on the two electronic PES's of a molecule in the condensed phase. By imparting a negative chirp on the pulse, we can enhance the ground-state coherent motion through a resonant impulsive stimulated Raman process, while a positive chirp has been shown to discriminate against such processes. From these simple experiments of changing the chirp of the excitation pulse, we have surmised that both S_0 and S_1 PES's of LD690 have level-dependent vibronic dephasing times, which vary from about 3 to <1 ps in the S_1 state and from >10 to about 1 ps in the S_0 state. The application of chirped pulse excitation to BR demonstrates significant suppression of the S_0 component in a photoreactive system by a PC pulse. Calculations for both LD and BR suggest that the use of shorter pulses with more well-defined chirps would improve selectivity, and it is possible that a short pulse with a small well-defined positive linear chirp could be used to excite wave packet motion only on the excited state, which could then be analyzed to provide information on the excited-state vibrational structure and dephasing. Negatively chirped pulses, on the other hand, may be useful for creating large-amplitude motion on ground-state potentials.[40,41] The use of more sophisticated pulse shaping techniques[42,43] can be expected to provide researchers with more opportunities to use tailored light fields to unravel molecular photophysics. Finally, these results demonstrate the dramatic effect of pulse phase structure on vibrational coherences observed in transient absorption experiments and suggest that caution should be used in the interpretation of such data when the excitation pulse is not well characterized.

References and Notes

(1) Baltuska, A.; Wei, Z. Y.; Pshenichnikov, M. S.; Wiersma, D. A. *Opt. Lett.* **1997**, *22*, 102.
(2) Nisoli, M.; De Silvestri, S.; Svelto, O.; Szipocs, R.; Ferencz, K.; Spielmann, C.; Sartania, S. Krausz. *Opt. Lett.* **1997**, *22*, 522.
(3) Fork, R. L.; Brito Cruz, C. H.; Becker, P. C.; Shank, C. V. *Opt. Lett.* **1987**, *12*, 483.
(4) Treacy, E. B. *IEEE J. Quantum Electron.* **1969**, *5*, 454.
(5) Melinger, J. S.; Ghandi, S. R.; Hariharan, A.; Goswami, D.; Warren, W. S. *J. Chem. Phys.* **1994**, *101*, 6439.
(6) Cerullo, G.; Bardeen, C. J.; Wang, Q.; Shank, C. V. *Chem. Phys. Lett.* **1996**, *262*, 362.
(7) Assion, A.; Baumert, T.; Helbing, J.; Seyfried, V.; Gerber, G. *Chem. Phys. Lett.* **1996**, *259*, 488.
(8) Kohler, B.; Yakovlev, V. V.; Che, J.; Krause, J. L.; Messina, M.; Wilson, K. R.; Schwenter, N.; Whitnell, R.; Yan, Y. J. *Phys. Rev. Lett.* **1995**, *74*, 3360.
(9) Bardeen, C. J.; Che, J.; Wilson, K. R.; Yakovlev, V. V.; Apkarian, V. A.; Martens, C. C.; Zadoyan, R.; Kohler, B.; Messina, M. *J. Chem. Phys.* **1997**, *106*, 8486.
(10) Jansky, J.; Adam, P.; Vinogradov, A. V.; Kobayashi, T. *Chem. Phys. Lett.* **1993**, *213*, 368.
(11) Averbukh, I.; Shapiro, M. *Phys. Rev. A* **1993**, *47*, 5086.
(12) Amstrup, B.; Szabo, G.; Sauerbrey, R. A.; Lorincz, A. *Chem. Phys.* **1994**, *188*, 87.
(13) Krause, J. L.; Whitnell, R. M.; Wilson, K. R.; Yan, Y. J.; Mukamel, S. *J. Chem. Phys.* **1993**, *99*, 6562.
(14) Scherer, N. F.; Carlson, R. J.; Matro, A.; Du, M.; Ruggerio, A. J.; Romero-Rochin, V.; Cina, J. A.; Fleming, G. R.; Rice, S. A. *J. Chem. Phys.* **1991**, *95*, 1487.
(15) Engel, V.; Metiu, H. *J. Chem. Phys.* **1994**, *100*, 5448.
(16) Lin, W. Z.; Fujimoto, J. G.; Ippen, E. P.; Logan, R. A. *Appl. Phys. Lett.* **1987**, *50*, 124.
(17) Nibbering, E. T. J.; Wiersma, D. A.; Duppen, K. *Phys. Rev. Lett.* **1992**, *68*, 514.
(18) Bardeen, C. J.; Wang, Q.; Shank, C. V. *Phys. Rev. Lett.* **1995**, *75*, 3410.
(19) Vos, M. H.; Rappaport, F.; Lambry, J. C.; Breton, J.; Martin, J. L. *Nature* **1993**, *363*, 320.
(20) Wang, Q.; Schoenlein, R. W.; Peteanu, L. A.; Mathies, R. A.; Shank, C. V. *Science* **1994**, *266*, 422.
(21) Zhu, L.; Sage, J. T.; Champion, P. M. *Science* **1994**, *266*, 629.
(22) Ruhman, S.; Kosloff, R. *J. Opt. Soc. B* **1990**, *7*, 1748.
(23) Tannor, D. J.; Rice, S. A. *J. Chem. Phys.* **1985**, *83*, 5013.
(24) Pollard, W. T.; Lee, S. Y.; Mathies, R. A. *J. Chem. Phys.* **1990**, *92*, 4012.
(25) Banin, U.; Bartana, A.; Ruhman, S.; Kosloff, R. *J. Chem. Phys.* **1994**, *101*, 8461.
(26) Shapiro, M.; Brumer, P. *J. Chem. Phys.* **1986**, *84*, 540.
(27) Dexheimer, S. L.; Wang, Q.; Peteanu, L. A.; Pollard, W. T.; Mathies, R. A.; Shank, C. V. *Chem. Phys. Lett.* **1992**, *188*, 61.
(28) Boyer, G.; Franco, M.; Chambaret, J. P.; Migus, A.; Antonetti, A.; Georges, P.; Salin, F.; Brun, A. *Appl. Phys. Lett.* **1988**, *53*, 823.
(29) Fragnito, H. L.; Bigot, J. Y.; Becker, P. C.; Shank, C. V. *Chem. Phys. Lett.* **1989**, *160*, 101.
(30) Foing, J. P.; Likforman, J. P.; Joffre, M.; Migus, A. *IEEE J. Quantum Electron.* **1992**, *28*, 2285.
(31) Albrecht, T. F.; Seibert, K.; Kurz, H. *Opt. Commun.* **1991**, *84*, 223.
(32) Bardeen, C. J.; Shank, C. V. *Chem. Phys. Lett.* **1993**, *203*, 535.
(33) Joo, T.; Albrecht, A. C. *Chem. Phys.* **1993**, *173*, 17.
(34) Yan, Y. J.; Mukamel, S. *J. Chem. Phys.* **1989**, *89*, 5160.
(35) Pollard, W. T.; Dexheimer, S. L.; Wang, Q.; Peteanu, L. A.; Shank, C. V.; Mathies, R. A. *J. Phys. Chem.* **1992**, *96*, 6147.
(36) Bardeen, C. J.; Shank, C. V.; *Chem. Phys. Lett.* **1994**, *226*, 310.
(37) Wise, F. W.; Rosker, M. J.; Milhauser, G. L.; Tang, C. L. *IEEE J. Quantum Electron.* **1987**, *23*, 1116.
(38) Miller, R. J. D. *Annu. Rev. Phys. Chem.* **1991**, *42*, 581.
(39) Mathies, R. A.; Brito Cruz, C. H.; Pollard, W. T.; Shank, C. V. *Science* **1988**, *240*, 777.
(40) Johnson, A. E.; Myers, A. B. *J. Chem. Phys.* **1996**, *104*, 2497.
(41) Hiller, E. M.; Cina, J. A. *J. Chem. Phys.* **1996**, *105*, 3419.
(42) Wefers, M. A.; Nelson, K. A. *J. Opt. Soc. Am. B* **1995**, *12*, 1343.
(43) Dugan, M. A.; Tull, J. X.; Warren, W. S. *J. Opt. Soc. Am. B* **1997**, *14*, 2348.